Journal of
NANOSTRUCTURES
JNS
NANOSTRUCTURES
JNS.kashanu.ac.ir

Fabrication of Novel High Potential Chromium-Doped TiO_2 Nanoparticulate Electrode-based Dye-Sensitized Solar Cell (DSSC)

A. Ehteram [a,*], M. Hamadanian [b,c], V. Jabbari [b]

[a] *Department of Electrical Engineering, Kashan Branch, Islamic Azad University, Kashan, IRAN*

[b] *Institute of Nanosciences and Nanotechnology, University of Kashan, Kashan, IRAN*

[c] *Department of Physical Chemistry, Faculty of Chemistry, University of Kashan, Kashan, IRAN*

Article history:
Received 14/10/2015
Accepted 19/11/2015
Published online 01/12/2015

Keywords:
$Cr@TiO_2$
Nanoparciculate Electrode
Charge Recombination
DSSC
Photovoltaic

**Corresponding author:*
E-mail address:
ehteram93@gmail.com
Phone: +98 31 55450460
Fax: +98 31 55540056

Abstract

In the current study, pure TiO_2 and Cr-doped TiO_2 ($Cr@TiO_2$) nanoparticles were synthesized via sol-gel method and the resulting materials were applied to prepare the porous TiO_2 electrodes for dye-sensitized solar cells (DSSCs). It is hypothesized that the advantages of the doping of the metal ions into TiO_2 lattice are the temporary rapping of the photogenerated electron-hole (charge carriers) by the metal dopants and the retarding charge recombination during electron migration from TiO_2 to the electrode surface. Spectroscopic and microscopic findings showed that all the prepared samples consist of only anatse phase with average size of 10-15nm. In addition, relative to the bare TiO_2, $Cr@TiO_2$ absorption in visible light region was considerably improved due to the surface Plasmon phenomenon. Current-voltage (I-V) curves exhibited that the solar cells made of $Cr@TiO_2$ nanoparticles results in higher photocurrent density than the cells made of bare TiO_2. The large improvement of photovoltaic performance of the Cr-doped TiO_2 cell stems from negative shift of TiO_2 conduction band and retarding charge recombination. Finally, it is concluded that the proposed route in the current study is an effective way to enhance the energy conversion efficiency and overall performance of DSSC.

1. Introduction

The charge separation plays an important role in determining energy conversion efficiency for producing solar fuels and solar electricity in dye solar cells [1, 2], photoelectrocatalysis [3] and photocatalysis systems [4]. As a key step in solar energy conversion, photogenerated electron-hole (e^-/h^+) pairs must be largely separated [5, 6].

Therefore, a deep understanding and controlling of charge separation process within photoexcited semiconductors is needed for the fabrication of a productive solar light energy conversion system.

TiO_2 is among the widely used material in solar energy applications such as photovoltaic solar cells [7, 8], water and air purification [9], and as UV absorbent in cosmetics [10]. It has been largely employed in bulk heterojunction solar cells (BHJ) and dye-sensitized solar cells (DSSC) in order to gain high energy conversion efficiencies along with low cost, easy fabrication, low level of toxicity, and a long-term stability [11]. However, the rapid recombination rate of electron-hole (e^-/h^+) on the TiO_2 nanoparticles limit to obtain high conversion efficiency for TiO_2 nanoparticle-based solar cells [6, 11]. Indeed, the injected electrons from sensitizer to the TiO_2 conduction band can react with oxidized sensitizer molecules and/or with the redox species in the electrolyte (Scheme 1).

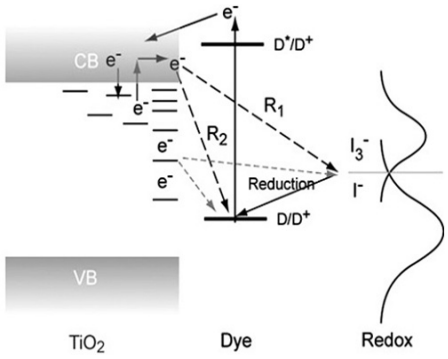

Scheme 1. The recombination (R) process within DSSC.

To retard the charge recombination within DSSC many efforts have been attempted such as the use of some novel dyes [12], core-shell structure [13, 14], and doping metal and nonmetal to improve the performance of DSSCs [15]. The incorporation of metal ion impurities into TiO_2 materials is very common approach to tailor electric conductivity or band gap for specific applications [16, 17]. Indeed, doping of TiO_2 with metals is one of the most suitable and effective way in order to extend the light absorption of TiO_2 and increase the lifetime of the electron-hole pair and thus to increase the efficiency of the photovoltaic performance.

Raftery et al., showed that doping of TiO_2 with metal could trap temporarily the photo-generated electrons (e^-) and holes (h^+), and thus suppress recombination of the charge carriers [18]. Zhang et al., found that cerium (Ce) doping could prevent the charge recombination of the photo-generated electrons and holes [19]. Imahori et al., fabricated Nb-, Ge-, and Zr-added TiO_2 composite electrodes in order to improve the overall performance of TiO_2-based DSSC. They reported that metal-doped TiO_2–based DSSC performance enhancement stem from TiO_2 conduction band negative shift [20]. Feng et al., found that doping of tantalum (Tl) into TiO_2 led to higher TiO_2–based solar cell efficiency [21]. They showed that DSSCs employing the Tl-doped TiO_2 results in a very high photovoltage of 0.87 V, which is very close to the theoretically predicted maximum. Some literatures reported that doping of Ni^{2+} ion could improves the photo-activity of TiO_2 due to the existence of Ni^{2+} suppresses charge recombination of e^-/h^+ pairs onto the TiO_2 surface [22, 23]. Mo et al. [24] found that TiO_2 doping with Fe^{3+}, Mo^{5+}, Ru^{3+}, Os^{3+}, Re^{5+}, V^{4+}, and Rh^+ at metal concentration range of 0.1%–0.5% considerably increased the photo-reactivity, but that Co^{3+} and Al^{3+} doping decreased the photo-reactivity. Ko et al., reported large improvement in energy conversion efficiency of TiO_2-based DSSC by doping of W and Al [25]. They exhibited that doping of Al into

the TiO_2 electrodes enhances photovoltage, but reduces photocurrent. In contrast, W-doped TiO_2 showed an opposite results.

The main purpose of the current study, which to best of our knowledge was done for the first time, is to study the effect of substituting Ti atoms of TiO_2 by Cr^{3+} ions via sol-gel method, which the resulting materials were used to fabricate anode electrode of DSSC via doctor blade technique. The current synthetic process can be readily extendable to permit doping of TiO_2 nanoparticles with different metals (e.g., Au, Fe, W, Ag); however, our study is limited to only Cr-doped TiO_2 system. The morphology, crystalline structure and other physicochemical characteristic of the prepared compounds were analyzed by SEM, TEM, EDX, XRD, FTIR, and UV-Vis DRS spectroscopy. The results illustrated that the doping of Cr^{3+} ions into TiO_2 largely influence physicochemical and photovoltaic properties of DSSCs. Finally, the photovoltaic performance of the different DSSCs were discussed and compared.

2. Materials and Methods

2.1. Chemicals

Titanium (IV) isopropoxide (TiP, Merck) of chemically pure reagent grade were used for preparing TiO_2 sol, acetic acid (Merck), $Cr(NO_3)_3$ (Merck), 4-tert-butylpyridine (4-tBP) (Aldrich), acetonitrile (Fluka), valeronitrile (Fluka), H_2PtCl_6 (Fluka), Iodine (I_2) (99.99%, Superpur1, Merck), lithium iodide (LiI) (Merck), ethyl celluloses (5–15 mPas at 5% in toluene:ethanol/80:20 at 25 ^{0}C), FTO glass (TEC-15 ohm, Dyesol) and Ru complex dye [cis-bis (isothiocyanato)bis(2,20-bipyridyl-4,40-dicar-boxylato)-ruthenium(II)bis-tetrabutyl ammonium: (N719), dyesol] were used as received. H_2O was purified by distillation and filtration (Milli-Q).

2.2. The Preparation of Cr-doped TiO_2 Nanoparticles

To synthesis Cr@TiO_2, TiP, ethanol and acetic acid with ratio of 1:2.5:2.5 were mixed together under ultrasonic reaction and the resulting solution was stirred for 3.0 h. To prevent the formation of TiO_2 precipitates, the pH of solution was controlled by acetic acid. Due to the ultrasonic waves contain high energy content, the large agglomeration of TiO_2 particles during their formation is suppressed. Afterwards, aqueous solution containing 5%mol $Cr(NO_3)_3$ was added to the mixed solution in drops. Finally, the mixed solution was placed into an oven to form wet gel. Then the wet gel was dried at 100 ◦C for 12.0 h to form dry gel powder. The dry gel powder was heated at 500 ◦C for 2.0 h in the muffle furnace and the nanosized Cr@TiO_2 powders were obtained after adequate rubbing.

2.3. Anode Electrode Preparation

Electrophoretic To make bare and Cr-doped TiO_2 paste, 15 g of ethyl celluloses (5–15 mPas at 5% in toluene:ethanol/80:20 at 25 ^{o}C, #46 070, Fluka) of 10 wt.% ethanolic mixture was added to a round bottomed rotavap flask containing 3g bare TiO_2 or Cr@TiO_2 and 10g of terpineol (anhydrous, #86480, Fluka) and diluted with 80 ml of ethanol. The resultant mixture was then sonicated using an ultrasonic horn (Sonics & Materials, Inc), alternating stirring, with a hand mixer (Ultraturrax, IKA), and sonication for three consecutive times. Water and ethanol were removed from the resulting solutions in a rotary evaporator (initial temperature 40°C). The final composition for doctor-blade deposition was 18

wt.% TiO_2, 9 wt.% ethyl cellulose and 73 wt.% terpineol. Then, one drop of $Cr@TiO_2$ sol (named $1Cr@TiO_2$), two drops of bare TiO_2 sol (named bare TiO_2), two drops of $Cr@TiO_2$ sol (named $2Cr@TiO_2$), four drops of $Cr@TiO_2$ sol (named $4Cr@TiO_2$) were doctor-bladed onto 4 cm^2 FTO glass substrates (sheet resistance = 15 ohm/square, Dyesol, Australia) to create a thin layer on FTO glasses. Then electrodes were first dried in an air oven at 80 ^{0}C for about 30 min and subsequently at 500 ^{0}C for 30 min to remove the organics.

The prepared films were immersed in a 0.3 mM N719 in ethanol solution overnight. The excess of N719 dye in the films was rinsed with anhydrous ethanol.

2.4. Solar Cells Assembly

The counter electrodes were platinized by spraying H_2PtCl_6 solution to TCO glass and annealed in air at 400 ^{0}C for 15 min. Then, the counter electrodes were placed directly on the top of the dye-sensitized films. The gap between the two electrodes was sealed by thermal adhesive films (Surlyn, Dupont). The electrolyte containing acetonitrile, I_2, LiI, and 4-tBP was filled from a hole made on the counter electrode, which was sealed by a cover glass and thermal adhesive films. The active electrodes area of DSCs was 0.25 cm^2. Thus, the typical sandwich type of DSCs was made (Scheme 2).

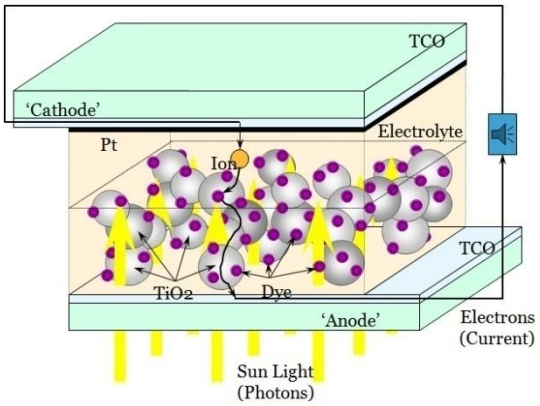

Scheme 2. Configuration of the manufactured DSC.

2.5. Spectroscopy Analysis

The X-ray diffraction patterns (XRD) were recorded on a Philips X'pert Pro MPD model X-ray diffractometer using Cu Kα radiation as the X-ray source. The diffractograms were recorded in the 2θ range of 20-80º. The morphology was revealed by a scanning electron microscope (SEM, Philips XL-30ESM, Holland) equipped with an energy dispersive X-ray detector (EDX, EDAX Genenis-4000, USA). UV-Vis DRS and UV-Vis absorption spectra were recorded by a Shimadzu 1800 spectrometer. Photovoltaic measurements employed an AM 1.5 solar simulator. The power of the simulated light was calibrated to be 100 $mWcm^{-2}$ by using a reference Si photodiode equipped with an IR-cutoff filter (KG-3, Schott), which was calibrated at three solar-energy institutes (ISE (Germany), NREL (USA), SRI (Switzerland)). I-V curves were obtained by applying an external bias to the cell and measuring the generated photocurrent with a Keithley model 2400 digital source meter. The voltage step and delay time of photocurrent were 10MV and 40 ms, respectively. Based on I–V curve, the fill factor (FF) is defined as:

$$FF = \frac{Pmax}{JSC \times VOC} = \frac{Jmax \times Vmax}{JSC \times VOC} \quad (1)$$

Where J_{max} and V_{max} are the photocurrent and photovoltage for maximum power output (P_{max}), J_{SC} and V_{OC} are the short-circuit photocurrent and open-circuit photovoltage, respectively. The overall energy conversion efficiency (η) is defined as:

$$\eta = J_{SC} \times V_{OC} \times FF / P_{in} \quad (2)$$

3. Results and Discussions

3.1. Crystalline Structure

Figure 1 shows XRD patterns of bare TiO_2 and Cr-doped TiO_2. All of the peaks in the samples are assigned to anatase phase [26]. No XRD pattern deriving from rutile phase is seen. Also, it must be noted that all the nanoparticles exhibit similar crystalline patterns. This confirms that anatase crystalline structure of TiO_2 was retained after doping of small amount of Cr^{3+} ions (5%mol) into TiO_2 structure. Furthermore, the XRD pattern did not show any metal or metal oxide phase and may be concluded that metal ions uniformly dispersed into the anatase TiO_2 crystallites.

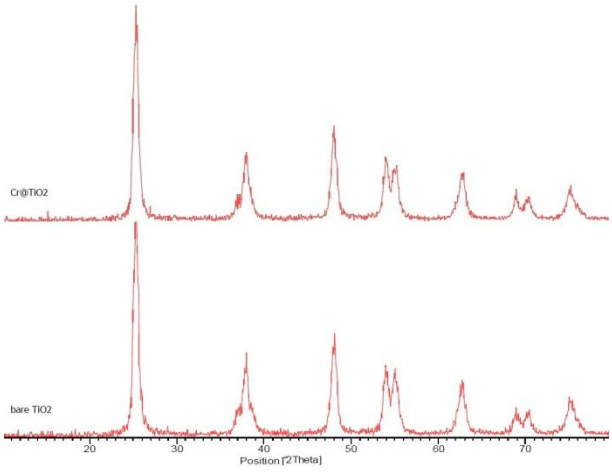

Fig. 1. XRD patterns of bare TiO_2 and Cr@TiO_2.

The particle size can be further estimated from the widths of the X-ray diffraction peaks using the Debye-Scherrer's equation: $d = k\lambda/\sqrt{A^2 - B^2}\cos 2\theta$, where d is the particle size, k = 0.9, λ is the wavelength of the X-ray (1.542 ˚A), θ is the diffraction angle, A is the width of the peak, and B is a background correction for the glass substrate (0.003 rad) [27]. Inserting the experimental data for a pronounced peak: 2θ = 25.45◦, A = 0.006283 rad, the average particle size d was 27 and 19 nm for bare TiO_2 and Cr@TiO_2, respectively.

3.2. Morphological and Elemental Analysis

Figure 2 exhibits the TEM images for the pure TiO_2 powders annealed at 500°C for 2 h. Roughly spherical TiO_2 particles are formed. The average size of the particles was about 20-30 nm [28].

EDX spectrum of Figure 3 provides the strong direct proof that Cr^{3+} ion is successfully doped within TiO_2 because characteristic peaks of the element Cr appears on the EDX spectrum [29].

SEM micrographs of the TiO_2 nanoparticles are shown in Figure 4. This images show global and uniform particles [30]. The observation indicates that the morphology of samples is very rough and may be beneficial to enhancing the adsorption of dye due to its great surface roughness and high surface area. The average diameter of the particles calculated from the micrograph also gives the value close to 20 nm.

The SEM micrograph of TiO_2 electrode made of bare TiO_2 nanoparticles annealed in 500 ^{0}C (Figure 5(a,b)) show a rough surface layer containing large TiO_2 chunks in which the individual TiO_2 particles are hardly visible [31]. The chunk structure is likely formed through the aggregation of TiO_2 arranged in a side-by-side configuration. Another possible reason for the appearance of irregular chunks on the TiO_2 layer is the stress-induced surface rumpling caused by

the fast cooling after 500 ^{0}C annealing [31]. Also, Figure 5(c,d) show the SEM micrograph of a cross-section of the TiO_2 photo-electrode which reveals the thickness of the fabricated electrode, where TiO_2 film with thickness about 12 micron lies on the top of FTO film. The image also shows that the electrode has nearly uniform thickness which is an important criterion to obtain good cells with high efficiency [31].

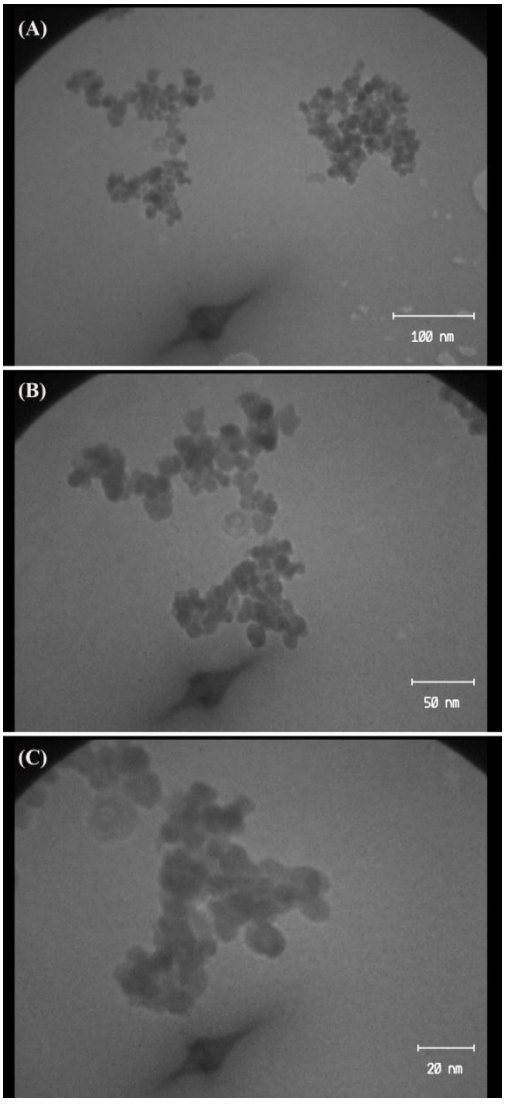

Fig. 2. TEM images of bare TiO_2 made with sol-gel method.

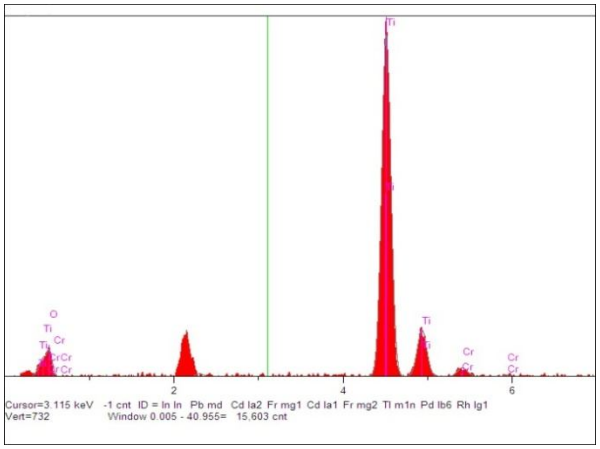

Fig. 3. EDX analysis of Cr@TiO_2.

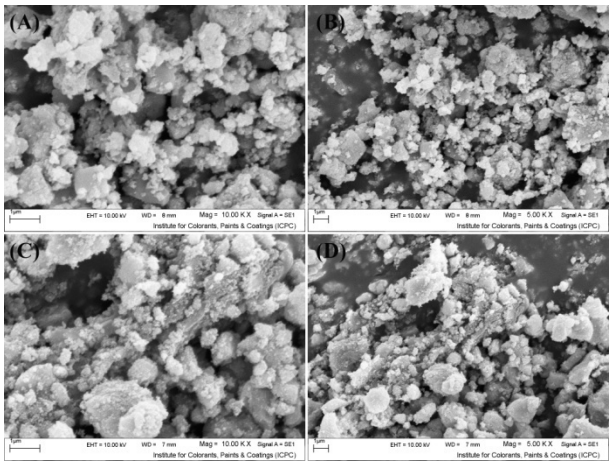

Fig. 4. SEM images of Cr@TiO_2 synthesized via sol-gel method in different magnifications.

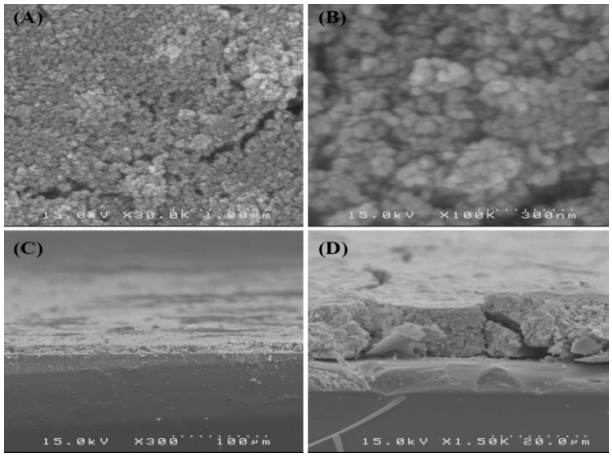

Fig. 5. SEM images of the electrode made of bare TiO_2 nanoparticles: surface (a,b) and cross-section view (c,d).

3.3. Band Gap Analysis by UV-Vis DRS Spectroscopy

The absorption spectra of bare TiO_2 and $Cr@TiO_2$ nanoparticles are recorded using UV–visible DRS spectrophotometer and the results are shown in Figure 6. The Figure 6 shows an absorption maximum around 320 nm which is usually attributed to charge transfer from TiO_2 valence band (VB) formed by 2p orbital of oxygen to the conduction band (CB) mainly formed by 3d t_2g orbital of Ti^{4+} cations [32]. Compared to the pure TiO_2, the absorption spectra of $Cr@TiO_2$ show an enhanced absorption in visible light region. Undoubtedly, the results reveal that the Cr^{3+} ions are incorporated into the TiO_2. The origin of the visible spectra of $Cr@TiO_2$ is due to formation of the dopant energy level within band gap of TiO_2 [32]. The electron transitions from the VB to the dopant energy level or from the dopant energy level to the CB can effectively result in the red shift in the TiO_2 band edge absorption threshold. [33].

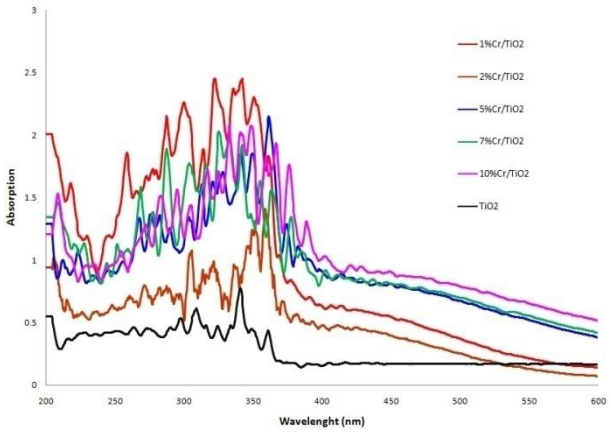

Fig. 6. UV-Vis DRS spectra of bare TiO_2 and $Cr@TiO_2$ nanoparticles.

The Kubelka–Munk functions were used to calculate the bare TiO_2 and $Cr@TiO_2$ nanoparticles band gap energy by plotting $[F(R)E]^{1/2}$ versus light energy. The optical absorption threshold of λ_g was estimated using the following equation, $\lambda_g = 1240/E_B$, where E_B is the TiO_2 band gap energy. The results showed that the band gap values of $Cr@TiO_2$ (<3.2 eV) was narrower than the pure TiO_2 (> 3.2 eV). Doping of Cr^{3+} presents a t_{2g} level of the 3d orbital of Cr^{3+} in the forbidden band of TiO_2, which provides $Cr@TiO_2$ an ability to absorb the photon with its wavelength longer than 400 nm. As a result, doping of Cr^{3+} ions promotes the separation of photogenerated holes and electrons of TiO_2, hence increases the photoreactivity of TiO_2 nanoparticles. Wang et al., have found that the DSSC made of photoelectrode with narrower band gap illustrates significant improvement in the overall energy conversion efficiency of DSSC [34]. So, it is expected that DSSC made of $Cr@TiO_2$ shows superior photovoltaic performance compared to DSSC made of bare TiO_2.

3.4. Chemical Structure Analysis by FTIR

FT-IR spectra (Figure 7) of pure TiO_2 and $Cr@TiO_2$ exhibit peaks corresponding to stretching vibrations of O–H and the bending vibrations of adsorbed water molecules around 3350–3450 and 1620–1635 cm^{-1}, respectively. The broad and intense band below 1200 cm^{-1} is ascribed to Ti–O–Ti vibration. Furthermore, surface hydroxyl groups of TiO_2 raise with metal doping, which is in favor of trapping photogenerated electrons to enhance the charge separation efficiency of electron–hole pairs [35]. The incorporation of the Cr^{3+} ions into TiO_2 does not show any further change in FT-IR spectra of TiO_2 which the result obtained are in consistent with the previous literature [36].

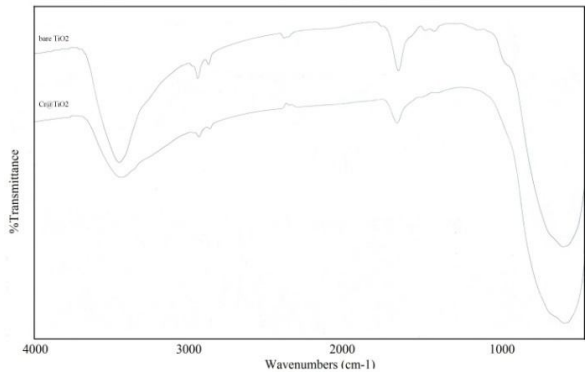

Fig. 7. FTIR analysis of bare TiO_2 and $Cr@TiO_2$ nanoparticles.

3.5. Photovoltaic Performance Analysis

To compare the photovoltaic performance, current-voltage (I-V) characteristics were analyzed using N719-sensitized electrodes made of pure TiO_2 and Cr-doped TiO_2, coupled with a platinum counter electrode under standard AM 1.5 (100 mW cm^{-2}) working conditions (Figure 8). Short-circuit current density (J_{SC}), open-circuit voltage (V_{OC}), fill factor (FF), and light-to-electricity energy conversion efficiency (η) values of the pure TiO_2, Cr-doped TiO_2 and P25 cells are also summarized in Table 1.

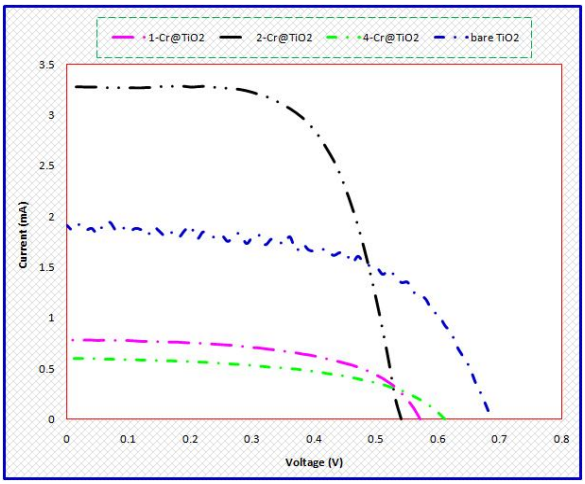

Fig. 8. Current-voltage **(**I–V) curves of DSSCs prepared using bare TiO_2, 1-$Cr@TiO_2$, 2-$Cr@TiO_2$ and 4-$Cr@TiO_2$ tested at 100mW/cm^2.

Table 1. Comparison results for 1 cm^2 active area DSSCs made of bare TiO_2 and Cr-doped TiO_2 working electrodes, tested under 100 mW.cm^{-2} AM1.5 simulated light.

No.	Cell type	Layers	I_{SC} (mA)[a]	V_{OC} (mV)[b]	η[c]
1	***bare TiO_2***	2	*1.91*	0.68	0.77
2	***1-Cr@TiO_2***	1	*0.78*	0.57	0.25
3	***2-Cr@TiO_2***	2	*3.30*	0.54	1.15
4	***4-Cr@TiO_2***	4	*0.60*	0.60	0.20

[a] J_{SC} is the short circuit current density.
[b] V_{OC} is the open circuit voltage.
[c] η is the overall conversion efficiency.

Charge recombination of electron-holes is one of the most important factors limiting DSSC overall performance. The doping of transition metals into the TiO_2 can considerably retard charge recombination at TiO_2/dye/electrolyte interface. Hence, the generation of O-Ti-Cr structure by metal doping could suppress reduction of the I_3^- ions onto TiO_2 electrode surface. Indeed, formation of the Ti–O–Cr inhibits the TiO_2 phase transition and blocks the Ti–O species at interface with the TiO_2 domains, and thus inhibiting agglomeration of TiO_2 particles and preventing the rutile growth [37]. Hence, entry of Cr^{3+} into the TiO_2 lattices suppresses the particle growth and consequently decreases the band gap values, which minimizes the charge (electron–hole) recombination, and as results, it is expected the $Cr@TiO_2$-based DSSC to show higher energy conversion efficiency compared to the pure TiO_2-based DSSC.

Our findings showed that J_{SC} and η were higher for the DSSC made of Cr-doped TiO_2 electrodes compared to DSSC made of bare TiO_2 electrodes. Moreover, we have found that the J_{SC} and η of Cr-doped TiO_2-based DSSC gradually increased with the raise of electrode film thickness, at maximum

reached for DSSC made of two layers doctor blade Cr@TiO_2, and then decreased with the further raise of the films thickness [38]. The benefit of transition Cr doping is the improved the trapping of electrons to inhibit electron-hole recombination during irradiation. For instance, to maintain charge neutrality, Cr^{3+} can act as photo-generated hole-trappers (Eqs. (1) and (2)), due to the energy level for Cr^{3+}/Cr^{4+} above valence band edge of the anatase TiO_2 (Scheme 3). It can reduce the number of electrons going from the TiO_2 semiconductor back to either the dye or the electrolyte.

$$TiO_2 + h\nu \rightarrow e_{cb}^- + h_{vb}^+ \quad (3)$$

$$Cr^{3+} + h_{vb}^+ \rightarrow Cr^{4+} \quad (4)$$

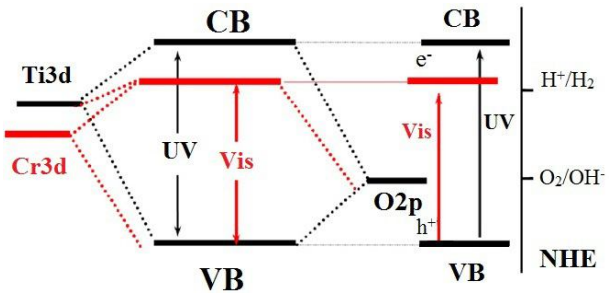

Scheme 3. The mechanism of effect of Cr^{3+} doping in shifting band-gap of TiO_2.

Another explanation is the fact that less the surface defect of TiO_2 the more absorption of dye molecule for an equal soaking time. Indeed, dye molecules prefer to attach the TiO_2 surface by chemisorption onto Ti^{4+} sites rather than onto Ti^{3+} due to Ti^{3+} instability [39]. Due to electroneutrality rule, Cr^{3+} ions prefer to replace Ti^{3+} rather than Ti^{4+} and it may be possible for Cr^{3+}-doped TiO_2 to have higher adsorbed dye molecules per unit area due to replacement of the Ti^{3+} by Cr^{3+} ions. Compactly absorbed dye molecules suppress tri-iodide ions to reach the TiO_2 surface because of steric hindrance. Also, the more dye adsorption means the more solar light harvest and consequently the more energy conversion efficiency.

In these experimental conditions, the J_{SC} of DSSC was small (3.3 mA) comparing to Gratzel's work [40, 41], which may be due to the poor electrolyte (in the latter, the electrolyte consists of LiI and I_2 solved into the solution containing ethylene carbonate and propylene carbonate which LiC ion plays an important role in increasing the J_{SC}), high ohm/square of conducting transparent glass (in latter, it was 8 ohm/square), imperfect solar cells design and the other factors. In our next work, we will work on optimum conditions in order to improve the photovoltaic performance of DSSCs.

4. Conclusion

In summary, for the first time we successfully analyzed the electrode physicochemical structures and photovoltaic performance of DSSCs made Cr-doped TiO_2 nanocomposite electrodes to reveal effects of partial Ti atom substitution by Cr^{3+} ions. The spectroscopic measurements showed that the bare TiO_2 and Cr-doped TiO_2 all contain only anatase phase and TiO_2 nanocrystalline structure was entirely retained after Cr^{3+} ions doping into TiO_2 structure, showing homogeneous distribution and replacement of Ti ions of TiO_2. In addition, our findings showed that the energy conversion efficiency of DSSC made of Cr@TiO_2 was largely higher compared to the bare TiO_2 under same working conditions due to retarding charge recombination by metal ions. Totally, our results demonstrated that a relatively small extent of metal retards the charge recombination of the photo-generated e^-/h^+ in TiO_2 which enhance the energy conversion efficiency of Cr@TiO_2-based DSSCs. This investigation contributes to the

understanding effects of the complex ion doping on TiO_2, and thus, provides a reference for improving its environmental application.

Acknowledgment

Authors are grateful to Council of Kashan Branch, Islamic Azad University, and Iran Nanotechnology Initiative Council for providing financial support to undertake this work.

References

[1] Hamadanian, M., Jabbari, V., Gravand, A., Asad, M. Surface & Coatings Technology, 206 (2012) 4531–4538.

[2] Tisdale, W. A., Williams, K., Timp, B., Science, 328 (2010) 1543–1547.

[3] Higashimoto, S., Sakiyama, M., Azuma, M., Thin Solid Films, 503 (2006) 201–206.

[4] Tachibana, Y., Vayssieres, L., Durrant, J., Nat. Photon., 6 (2012) 511–518.

[5] Kudo, A., Miseki, Y., Chem. Soc. Rev., 38 (2009) 253–278.

[6] McFarland, E. W., Tang, J., Nature, 421 (2003) 616–618.

[7] Bakulin, A. A., Rao, A., Pavelyev, V. G., Science, 335 (2012) 1340–1344.

[8] Grätzel, M., Journal of Photochemical and Photobiology: Photochemical Reviews, 4 (2003) 145–153

[9] Kabra, K., Chaudhary, R., Sawhney, R.L., International Journal of Green Energy, 6 (2009) 83-91.

[10] Jaroenworaluck, A., Sunsaneeyametha, W., Kosachan, N., Stevens, R., 38 (2006) 473-477.

[11] Wang, M., Huang, C., Cao, Y., Yu, Q., Deng, Z., Journal of Physics D: Applied Physics, 42 (2009) 155104-155110.

[12] Karthikeyan, C. S., Katja, P., Wietasch, H., Thelakkat, M., Sol. Energy Mater. Sol. Cells, 91 (2007) 432–439.

[13] Zaban, A. S., Chen, G., Chappel, S., Gregg, B. A., Chem. Commun., 12 (2000) 2231–2232.

[14] Chappel, S., Chen, S. G., Zaban, A., Langmuir, 18 (2002) 3336–3342.

[15] Ma, T., Akiyama, M., Abe, E., Imai, I., Nano Lett., 5 (2005) 2543–2547.

[16] Stamplecoskie, K. G., Ju, J., Farvid, S. S., Radovanovic, P. V., Nano Lett., 8 (2008) 2674–2681.

[17] Perea, D. E., Hemesath, E. R., Schwalbach, E. J., Lensch-Falk, J. L., Voorhees, P. W., Lauhon, L., J. Nat. Nanotechnol., 4 (2009) 315–319.

[18] Klosek, S., Raftery, D., J. Phys. Chem. B, 105 (2001) 2815-2821.

[19] Zhang, X., Liu, Q.Q., Mater. Lett., 62 (2008) 2589-2593.

[20] Imahori, H., Hayashi, S., Umeyama, T., Eu, S., Oguro, S., Kang, A., Matano, Y., Shishido, T., Ngamsinlapasathian, S., Yoshikawa, S., Langmuir, 22 (2006) 11405-11411.

[21] Feng, X., Shankar, K., Paulose, M., Grimes, C. A., Angew. Chem. Int. Ed., 48 (2009) 8095–8098.

[22] Kim, D. H., Choi, D. K., Kim, S. J., and Lee, K. S., Catalysis Communications, 9 (2008) 654–657.

[23] Dhayal, M., Sharma, S. D., Kant, C. K., Saini, K., and Jain, S. C., Surface Science, 602 (2008) 1149–1154.

[24] Mo, J., Zhang, Y., Xu, Q., Lamson, J. J., Zhao, R., Atmospheric Environment, 43 (2009) 2229–2246.

[25] Ko, Y K. Lee, H., Jung, C. Y., J. Journal of Colloid and Interface Science, 283 (2005) 482–487.

[26] Hamadanian, M., Jabbari, V., Asad, M., Shamshiri, M., Mutlay, I., Journal of the Taiwan

Institute of Chemical Engineers, 44 (2013) 748–757.
[27] Hamadanian, M., Sadeghi Sarabi, A., Mihammadi Mehra, A., Jabbari, V., Applied Surface Sciences, 257 (2011) 10639–10644.
[28] Hamadanian, M., Jabbari, V., Gravand, A., Materials Science in Semiconductor Processing, 15 (2012) 371–379.
[29] Hamadanian, M., Reisi-Vanani, A., Razi, P., Hoseinifard, S., Jabbari, V., Applied Surface Science, 285 (2013) 121–129.
[30] Hamadanian, M., Sadeghi Sarabi, A., Mihammadi Mehra, A., Jabbari, V., Journal of Materials Science in Semiconductor Processing, 21, (2014) 161-166.
[31] Hamadanian, M., Jabbari, V., Gravand, A., Materials Science in Semiconductor Processing, 16 (2013) 1352–1359.
[32] Nagaveni, K., Hegde, M.S., Madras, G., J. Phys. Chem. B, 108 (2004) 20204.
[33] Choi, W., Termin, A., Hoffmann, M.R., J. Phys. Chem., 98 (1994) 13669.
[34] Wang, X., Yang, Y., Jiang, Z., Fan, R., Eur. J. Inorg. Chem., 12 (2009) 3481–3487.
[35] Wang, Y.M., Liu, S.W., Lu, M.K., Wang, S.F., Gu, F., Gai, X.Z., Cui, X.P., Pan, J., J. Mol. Catal. A, 215 (2004) 137-142.
[36] Lam, C., Chiang, K., Amal, R., Gary, K., Low, C., Appl Catal B Environ., 72 (2006) 364-370.
[37] Zhang, Y., Zhang, H., Xu, Y., Wang, Y. J., Solid State Chem., 177 (2004) 3490–3498.
[38] Wang, Y., Hao, Y., Cheng, H., Ma, J., Xu, B., Li, W., Cal, S., Journal of Materials Science, 34 (1999) 2773–2779.
[39] Murakoshi, K., Kano, G., Wada, Y., Yanagida, S., Miyazaki, H., Matsumoto, M., Murasawa, S., J. Electroanal. Chem., 396 (1995) 27-34.
[40] Oregan B. O., and Gratzel, M., Nature, 353 (1991) 737–739.
[41] Nazeeruddin, M. K., Kay A., and Gratzel, M., J. Amer. Chem. Soc., 115 (1993) 6832-6838.